scientific reports

Check for updates

OPEN

Design and development of different adaptive MPPT controllers for renewable energy systems: a comprehensive analysis

Bongani Eswaraiah & Kethineni Balakrishna✉

As of now, all over the world is focusing on the Electric Vehicle (EV) technology because its features are low environmental pollution, less maitainence cost required, high robustness, and good dynamic response. Also, the EVs work continuously until the input fuel is provided to the fuel stack. Here, a Proton Exchange Membrane Fuel Cell (PEMFC) is used as an input source to the electric vehicle system because of its merits fast startup, and quick response. However, the PEMFC gives nonlinear voltage versus current characteristics. As a result, the extraction of maximum power from the fuel stack is very difficult. The main aim of this work is to study different Maximum Power Point Tracking Techniques (MPPT) for the DC-DC converter-fed PEMFC system. The studied MPPT controllers are Adjusted Step Value of Perturb & Observe (ASV with P&O), Adaptive Step Size with Incremental Conductance (ASS with IC), Radial Basis Functional Network (RBFN), Incremental Step-Fuzzy Logic Controller (IS with FLC), Continuous Step Variation based Particle Swarm Optimization (CSV with PSO), and Adaptive Step Value-Cuckoo Search Algorithm (ASV with CSA). The selected MPPT controllers' comprehensive study has been in terms of maximum power extraction, tracking speed of the MPP, settling time of the fuel stack output voltage, oscillations across the MPP, and design complexity. From the comprehensive performance results of the hybrid MPPT controllers, the ASV with CSA technique gives superior performance when equated to the other MPPT controllers.

Keywords Accuracy of MPP, Converter duty cycle, DC-DC converter, Efficiency of the MPPT controller, Fast MPP tracking speed, Plus oscillations across the functioning point of the fuel stack

As of now, the nonrenewable energy sources utilization kept on reducing because of their drawbacks are more implementation costs, excessive environmental pollution, and heavy damage to human health, wildlife, and habitat loss[1]. Also, nonrenewable energy sources require a high catchment area for the installation and release the greenhouse gasses[2]. So, most of the automotive industries are working on the development of various renewable energy systems. The most popularly used renewable energy systems are wind, solar, tidal, hydropower, and geothermal energy[3]. In wind power generation systems, the kinetic energy of the wind blades is converted into an electrical power supply by using the Permanent Magnet Synchronous Generator (PMSG). After collecting the electricity from the PMSG, the power converters are utilized for the conversion of direct power supply into alternative power supply. In addition, the transformer is included with power converters for enhancing the voltage profile of the grid. The features of wind power systems are very low operating cost, clean energy, effective utilization of land space, and creating more jobs for human beings[4]. The drawbacks of wind systems are noise pollution, intermittent, high environmental impact, and suitable only at remote locations. The demerits of wind power production systems are limited by utilizing the solar energy source[5].

The solar cells convert the sunlight photo energy into useful electrical power. Every cell gives only 0.78–0.95 V which is not useful for local load applications[6]. So, the solar cells are integrated in parallel and series sequence to improve the supply power rating of the solar system. The working nature of solar cells is quite equal to the P-N diode operation. The features of solar systems are diverse applications, reduced electricity bills, less maitainence cost, plus ease of maintenance[7]. The drawbacks of this power generation system are weather dependent, needs a high catchment area for installation, and its working performance depends on environmental pollution. So, the above drawbacks of solar, and wind energy systems are limited by using fuel cell technology[8]. A fuel stack is a device that transfers chemical energy into an electrical power supply by the use of electrochemical reactions.

Vignan's Foundation for Science Technology and Research, Vadlamudi, India. ✉email: kbk_eee@vignan.ac.in

In the fuel cell, the oxygen and hydrogen atoms are reacted with each other and generate power along with the water and heat as the byproducts[9]. The fuel cells give very little pollution and also give more than two times the efficiency of the other renewable energy systems. Based on the operating temperature, the fuel cells are classified as low operating temperature (25–100 °C) fuel cells, medium operating temperature fuel cells (100–500 °C), plus high operating temperature fuel cells (500–1000 °C).

For all the types of fuel stacks, the utilized input fuels are hydrogen, low hydrocarbons, alcohols, hydrazine, metal hydrides, and high hydrocarbons. The supplied input fuel is oxidized at the anode chamber, and the oxidant is reduced at the cathode side. Inside the fuel stack, one species of ions is shifted from anode to cathode via electrolyte to combine these with their counterparts[10]. The available electrons flow through the external circuit to generate the electrical current. In[11], based on the type of electrolyte, the researchers explained the different categories of fuel stacks which are Solid Oxide Fuel Stack (SOFS), Molten Carbonate Fuel Stack (MCFS), Alkaline Fuel Stack (AFS), and Phosphoric Acid Fuel Stack (PAFS). Certain solid material has the property to conduct electricity at very high temperatures and it works as an electrolyte for the solid oxide-based fuel stack. In[12], the authors selected the SOFS for supplying the power to the auxiliary power storage application. High operating temperature-based solid oxide cells give pollution-free, and clean energy to supply the electrical energy to the local consumers with high operating efficiency[13]. The merits of this solid oxide cell over traditional power supply systems are high reliability, modularity, high input fuel adaptability, and good functioning efficiency. Also, this fuel cell releases very less amount of nitrous oxide and solid dioxide.

Here, due to the high temperature withstand stability of the solid oxide fuel cell, the natural gas is formed inside the fuel stack. As a result, the expensive external reformer is not required in the SOFS. The high-operating pressurized SOFS is used as a combustor in the gas power generation system. The SOFS-based gas turbine electricity supply network's maximum functioning efficiency is 70%. In[14], the researchers developed the advanced solid oxide cell which is a combination of sealing fewer properties of a tubular cell with integral ribs, and a flatted air electrode. This tubular cell-based SOFS consists of a concise current path. So, the resistance of the solid oxide cell is very low, and more output power over the other fuel cells. The main feature of SOFS is noise-less operation. The drawback of SOFS is high startup time because of its high operating temperature[15]. As a result, many chemical and mechanical compatibility issues occur in the solid oxide cell. The applications of solid oxide fuel cells are emergency backup power supply, transportation systems, submarine systems, and rockets. Also, most of the utility vehicles are implemented by utilizing the solid oxide membrane-based fuel stack[16].

From the literature study, the reduction of carbon footprint utilization has been done by using molten carbonate fuel cells[17]. Due to this MCFS, the amount of carbon dioxide released from nonrenewable energy sources is reduced. The features of MCFS are highly efficient, and cleaner over to the traditional power supply networks. Also, most of the MCFS are used in stationary applications because of their compact, less noise pollution. In[18], the authors studied the photovoltaic systems along with the MCFS for generating power for all local consumers. Here, the power is equally shared along with the inverters and step-up transformers. This hybrid power network is useful for supplying continuous power to all hospitals as well as shopping malls. In this hybrid power system, the per-unit cost of the solar system is two times of the MCFS power supply. Also, the molten carbonate cell gives slightly higher profits when equated to the solar modules. However, the reduction of operational, and maitainence costs is a challenging task in the MCFS. Also, the natural gas price in the MCFS is very high. To overcome the disadvantages of molten carbonate cells, in[19], the researchers used the PAFS along with the solar, plus wind power system for supplying the power to the microgrid network. Phosphoric acid cells a one of the most popular fuel stacks that are used for food drier systems to protect the food from various chemicals[20]. In this PAFS, the electrolyte is developed with highly concentrative phosphoric acid along with the silicon carbide. The functioning temperature of this cell is between 150 and 210 °C. The electrodes of the PAFS are developed by utilizing the carbon cloth coating. Finally, the dispersed catalyst is used in the PAFS.

The phosphoric acid fuel cells are used in 100–400 kW stationary applications, backup power supply for industrial as well as commercial applications, residential buildings, and remote accessible areas[21]. The demerits of PAFS are less power density and a very aggressive electrolyte. Also, the PAFS works with very high startup time. As a result, this fuel stack is not useful for emergency power applications. The disadvantages of PAFS are limited by utilizing the AFS. The alkaline cells are anionic exchange membrane fuel cells that are used to replace the liquid electrolyte alkaline cells. Also, different manufacturers developed advanced alkaline catalyst material that has high thermal stability and gives very good performance[22]. The peak current density and power density of alkaline fuel stacks are 100–300 mA/cm^2, and 50–300 mW/cm^2 respectively. The lifetime of this fuel cell is greater than 5000 h, and its degradation rate is 3–20 $\mu V/h$[23].

Here, the anode of the alkaline fuel stack is designed by using platinum, and nickel. Similarly, the cathode is implemented by utilizing the Manganese dioxide. At the anode, the platinum catalyst breaks the alkaline liquid into alkaline ions for supplying the electricity to the external load circuit, and the nickel cathode collects the anode ions which are converted into waste chemicals. The features of alkaline fuel stacks are less operating temperature capability, easy handling, and very good operating efficiency[24]. Also, this AFS is used in the Apollo space mission application. The disadvantages of AFS are high manufacturing cost, and lack of infrastructure to support the hydrogen distribution. However, the above fuel cell drawbacks are overcome by using the PEMFS. The attractive features of PEMFS are fast startup and quick response[25].

The polymer membrane fuel stacks give nonlinear voltage versus current characteristics[26]. Also, the functioning point of the fuel stack changes from one point to another point on the V-I characteristics of the fuel stack at different water membranes, and operating temperature conditions. So, the peak power extraction from the fuel stack is highly difficult. At this time, the MPPT controller plays an important role in stabilizing the maximum power point of the fuel stack at various water membrane conditions[27]. As a result, the overall fuel stack system supplies constant power to the electric vehicle load. From the previously published articles, the MPPT technologies are differentiated as traditional, artificial intelligence, metaheuristics, and soft computing

methods. The most popular traditional MPPT technologies are Perturb & Observe (P&O)[28], fractional current, Incremental Conductance (IC)[29], fractional voltage, Incremental Resistance (IRR), and Ripple Correlation Method (RCM). In[30], the researchers utilized the P&O concept for a standalone DC–DC converter-fed fuel array system to vary the duty cycle of the interleaved converter thereby enhancing the load voltage profile of the electric vehicle system. Here, the P&O is investigated along with the Proportional and Integral (PI) controller in terms of steady-state oscillations of the fuel cell output voltage, converter voltage gain, and oscillations of MPP under different water membrane conditions of the fuel stack. From the simulation results, the authors concluded that the P&O methodology gives better performance when equated to the PI controller.

Similarly, in[31], the researchers introduced the drift-free P&O controller for improving the voltage extraction capability of the fuel stack at dynamic water membrane conditions. The P&O controller tracks the MPP by equating the instantaneous slope value of the V–I curve with the previously stored slope value. The comparative slope value consists of a positive indication then the perturbation moves in the front direction. Otherwise, the perturbation of the P&O controller moves in the backward direction. This process continues until the functioning point of the fuel stack comes to the one stable position on the V–I curve of the fuel stack. However, this MPPT method does not give an accurate MPP position and also gives an oscillated MPP position because of the improper decision made by the P&O controller at dynamic operating water membrane conditions of the fuel stack[32]. So, the drift-free P&O methodology is used in the 100 W standalone fuel stack system to eliminate the disadvantages of a basic P&O controller. The drawbacks of drift-free P&O methodology are less convergence speed and more time for reducing the oscillations of MPP. So, the fractional current power point tracking controller is used in the PV/PEMFS hybrid power generation system for identifying the functioning point of the overall power supply network[33]. The merits of this controller are fast-tracking speed, very low cost, easy handling, and very good static response. But it gives a less accurate MPP position. So, the entire system gets affected by the heat and conduction losses.

The fractional voltage-based PI controller is utilized in the hybrid grid-connected fuel stack system to maintain the voltage stability of the grid at diverse water membrane conditions of the fuel stack system[34]. In this method, a separate switch is required for evaluating the open circuit voltage of the fuel stack. Here, the open circuit fuel stack voltage is measured by the shutdown of the entire system. As a result, the hybrid system gives a very bad dynamic response. So, the IRR MPPT concept is used in the article[35] for reducing the oscillations of MPP. In this method, the current density function is utilized for moving the functioning point of the fuel stack near the actual MPP position[36]. At the starting point of the fuel stack V–I curve, the variation of the current density value is positive then the functioning point of the fuel stack goes in the forward direction. If the operating point of the fuel stack reaches the global MPP position then the current density function value is zero. The merits of an IRR controller are fast static and dynamic response when equated to the traditional MPPT techniques[37]. The fuel stack-fed multiphase DC-DC converter circuit generates fluctuated output current ripples and voltage ripples which are sent to the RCM block for identifying the suitable operating duty cycle of the DC-DC converter. Due to this controller operation, the entire system's heat conduction losses are reduced. As a result, the operating and maitainence costs of the fuel stack are reduced extensively[38]. The drawbacks of this controller are less applicable for quick changes in the operating temperature conditions of the fuel stack and needs high space for installation.

The fractional order variable step value-based IC power point identifier is applied to the PEMFS power supply system for effective tracking of the fuel stack MPP. Here, the main aim of the variable step fractional order IC controller is improving the steady state as well as dynamic response of the PEMFS at quick changes in water membrane conditions[39]. The merits of this controller are good tracking speed, a smaller number of sensing devices required for sensing the fuel stack parameters, and extracting the maximum power of the fuel stack thereby enhancing the overall system efficiency. As a result, the PEM fuel stack system input fuel utilization is reduced. So, this controller reduces the maintenance and installation cost of the entire power supply network[40]. The Hill Climb Controller (HCC) working is quite similar to the large perturbation size-based P&O method. Here, in this HCC, there are different perturbation step size values are selected which are the high perturbation step, and the low perturbation step. The high perturbation step concept is utilized at the beginning stage of the HCC operation to enhance the convergence speed of the controller[41]. After that, the perturbation step value is reduced to eliminate the distortions of converter output voltage. The disadvantages of these traditional controllers are less MPP tacking speed, and may not be applicable for quick changes of water membrane conditions of the fuel stack.

In[42], the authors focused on the conventional neural network controller for estimating the fuel stack output power thereby generating the suitable duty cycle to the three-phased z-source power converter. Here, the input signals fed to the artificial intelligence controller are oxygen consumption, hydrogen decomposition, utilized temperature, and the Faraday constant of the fuel stack. The features of neural network-based MPPT controllers are fast response, required less formal statistical training, and the capability to handle highly complex nonlinear issues. However, the neural network drawbacks require high training time, plus highly knowledgeable candidates are required to operate the controller[43]. In this work, there are various types of hybrid MPPT controllers are studied for generating the optimum duty cycle to the conventional boost converter and which are compared in terms of fuel stack output voltage, converter output voltage, fuel stack output current, converter output current, the efficiency of MPPT controller, settling time of the load voltage, number iterations required to track the MPP, and design complexity of the controller[44]. Here, these hybrid controllers overcome the disadvantages of traditional, and soft computing controllers. The detailed differentiation of all types of MPPT methodologies is illustrated in Fig. 1 The utilized fuel module technology is mentioned in Fig. 2.

The fuel stack gives very high-level output currents. Due to this, the system power conduction losses are increased extensively[45]. So, there are various categories of power DC–DC converters are used to improve the voltage profile rating of the induction motor-fed fuel stack system[46]. The major classification of power converters

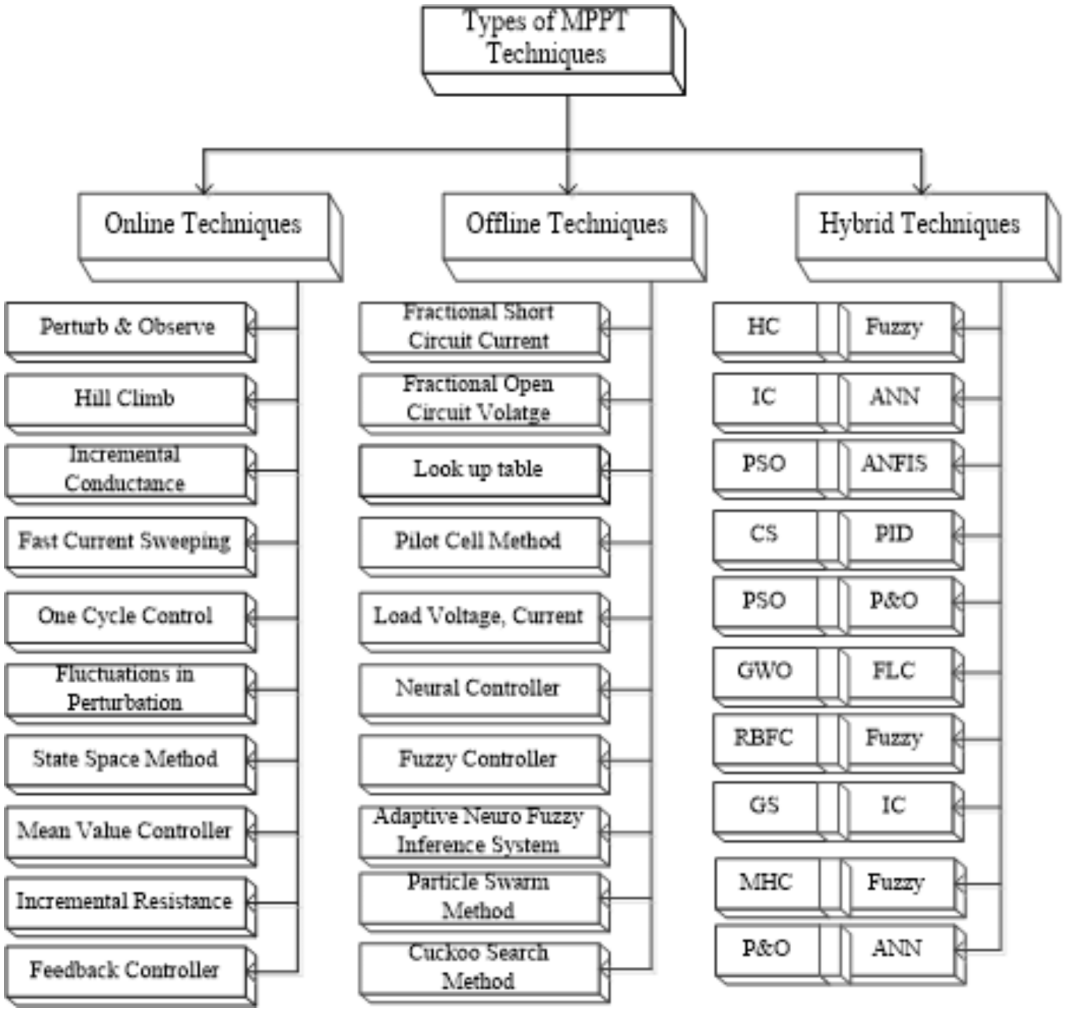

Fig. 1. Types of power point identifying controllers for PEMFC.

are non-isolated, and isolated power converters. All the isolated converters needed separate transformers, and rectifiers. In addition, these converters needed more space for installation. Also, the manufacturing cost of the isolated converters is very high. From the literature survey, the generally isolated converters consist of an output load that is separated from the input signal and are classified as bridge-type forward converters and flyback converters[47]. In a forward converter, the load voltage gain mainly depends on the input transformer. The features of a forward converter are galvanic isolation, multiple outputs, and the ability to provide low as well as high output voltage supplies simultaneously. However, the major disadvantage is the high cost of implementation. In the article[48], the authors referred to the flyback technology for DC–DC power conversion. The flyback converter is capable of accommodating the non-isolated and isolated formations. However, the drawbacks of the isolated converter are less operating efficiency, very high leakage current, and high sensitivity to operating temperature. So, in this work, a conventional non-isolated DC–DC converter is utilized for optimizing the overall cost of the PEMFS-fed non-isolated converter system. The features of this converter are less space required for installation, more efficiency, and high flexibility.

Mathematical implementation of PEM fuel stack

Present non-renewable sources reduction, and environmental considerations, the fuel cell stacks are acting as renewable energy systems for supplying electricity to electric vehicle systems. Most of the fuel stacks' input source is H_2 which is produced from the various biological sources[49]. The major H_2 production methodologies are steam reforming of CH_4 and Coke. In steam reforming of methane, the CH_4 chemical is reacted with the water at 800 °C[50]. As a result, the hydrogen, plus carbon monoxide chemical compounds are generated. The combined chemical composition of hydrogen and carbon monoxide is sent to the cooling compression chamber to separate the pure hydrogen content. Similarly, in the steam reforming of coke, the coke is combined with the water in the presence of nickel catalyst at 1000 °C to produce the carbon monoxide, and hydrogen[51]. The general features of hydrogen are tested less, odorless, colorless, and lightweight gas.

In this work, the PEMFC is used as a source for the electric vehicle load. The input source of PEMFC is hydrogen which is sent to the anode of the fuel stack. The proton-conducting polymer is worked as an electrolyte

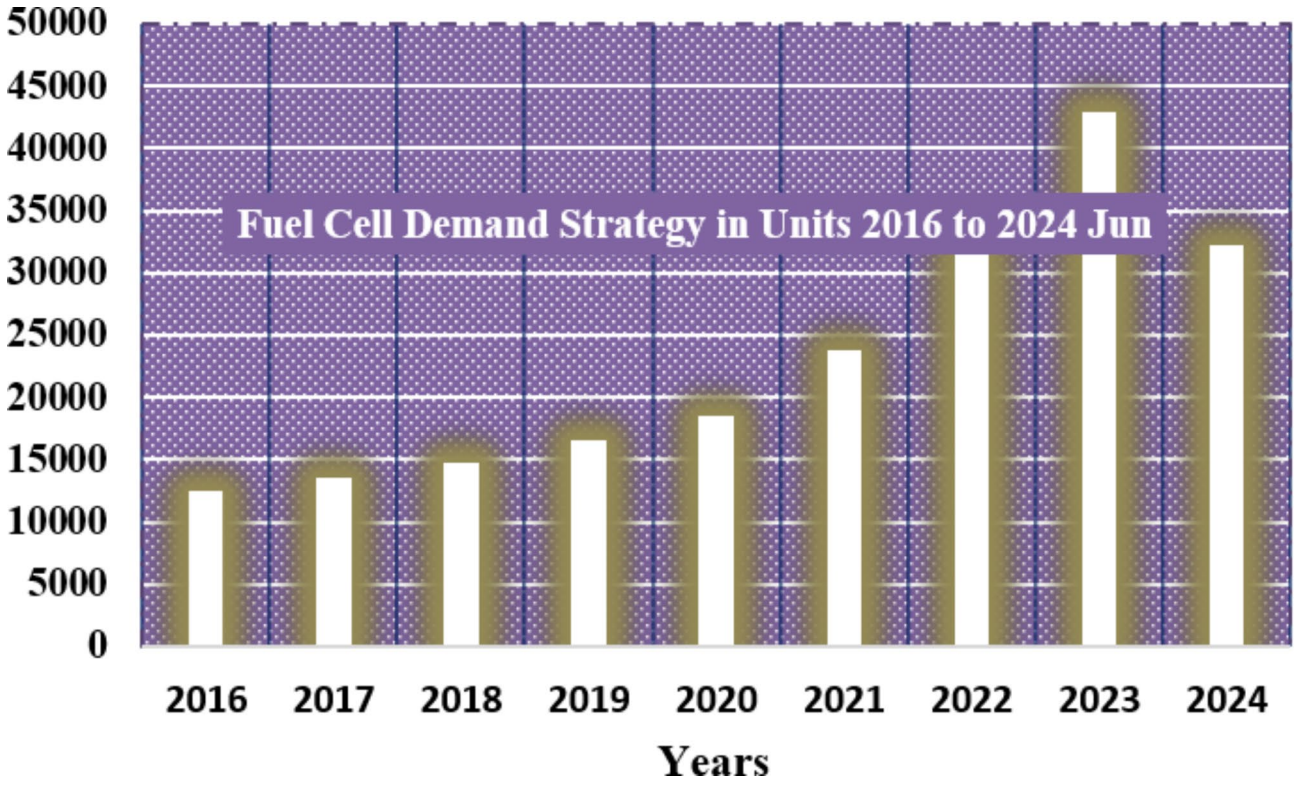

Fig. 2. Detailed utilization of polymer cell under quick variation of temperatures.

in the PEMFS. The chemical reactions of the polymer membrane fuel stack are explained in Fig. 3(a), and its resultant circuit is given in Fig. 3(b). The PEMFS is designed by using the polymer membrane electrolyte. The utilized electrolyte consists of different layers which are diffusion layer, catalyst layer, anode, plus cathode chambers. In this fuel stack, the paper-type carbon is covered by both anode and cathode electrodes to protect the PEMFS from the higher operating temperature conditions. The major observation of this fuel stack is polymer membrane is not conducting electrically. Also, the PEMFS works at 100 °C temperature for the effective utilization of the hydrogen.

From Fig. 3(a), the direct combination of O_2, and H_2 generates the heat energy. Here, the hydrogen moves near the anode chamber and it separates into hydrogen ions and electrons. The resultant hydrogen ions move from the anode chamber to the cathode chamber. The available electrons in the PEMFS are collected by using an external circuit. The proposed PEM fuel stack chemical reactions are derived as,

$$H_2 \rightarrow 2H^+ + 2e^- \tag{1}$$

$$2H^+ + 2e^- + \frac{1}{2}O_2 \rightarrow H_2O \tag{2}$$

$$H_2 + \frac{1}{2}O_2 \rightarrow H_2O + E \tag{3}$$

From the equivalent circuit of the fuel stack, the single cell output voltage is represented as V_{FC} which mainly depends on the three types of fuel stack resistors which are concentrative (R_{Co}), active polarization resistors (R_{Ac}) plus ohmic resistors (R_{Oh}). The voltage drops across the three resistors, and the open circuit voltage of the fuel stack is represented as active voltage (V_{Ac}), ohmic voltage (V_{Oh}), concentrated voltage (V_{Co}), and thermodynamic voltage (V_{otv}). Finally, there is a total N number of fuel cells interconnected to generate the high output voltage which is represented as V_{total}.

$$V_{total} = N{*}V_{FC} \tag{4}$$

$$V_{FC} = V_{0tv} - V_{Oh} - V_{Co} - V_{Ac} \tag{5}$$

$$V_{Otv} = 1.29 - 0.8e^{-3}\,(T_{Fop} - 298.12) + 4.3e^{-5}\mathrm{In}(P_{H_2}\sqrt{P_{O_2}})T_{Fop} \tag{6}$$

$$P_{H_2} = \frac{1}{2}HV_A{*}P^{sat}_{H_2O}\left(\frac{1}{\frac{HV_A{*}P^{sat}_{H_2O}}{P_A}\exp\left(\frac{1.65(I_{cell}/A)}{T_{Fop}}\right)}\right) \tag{7}$$

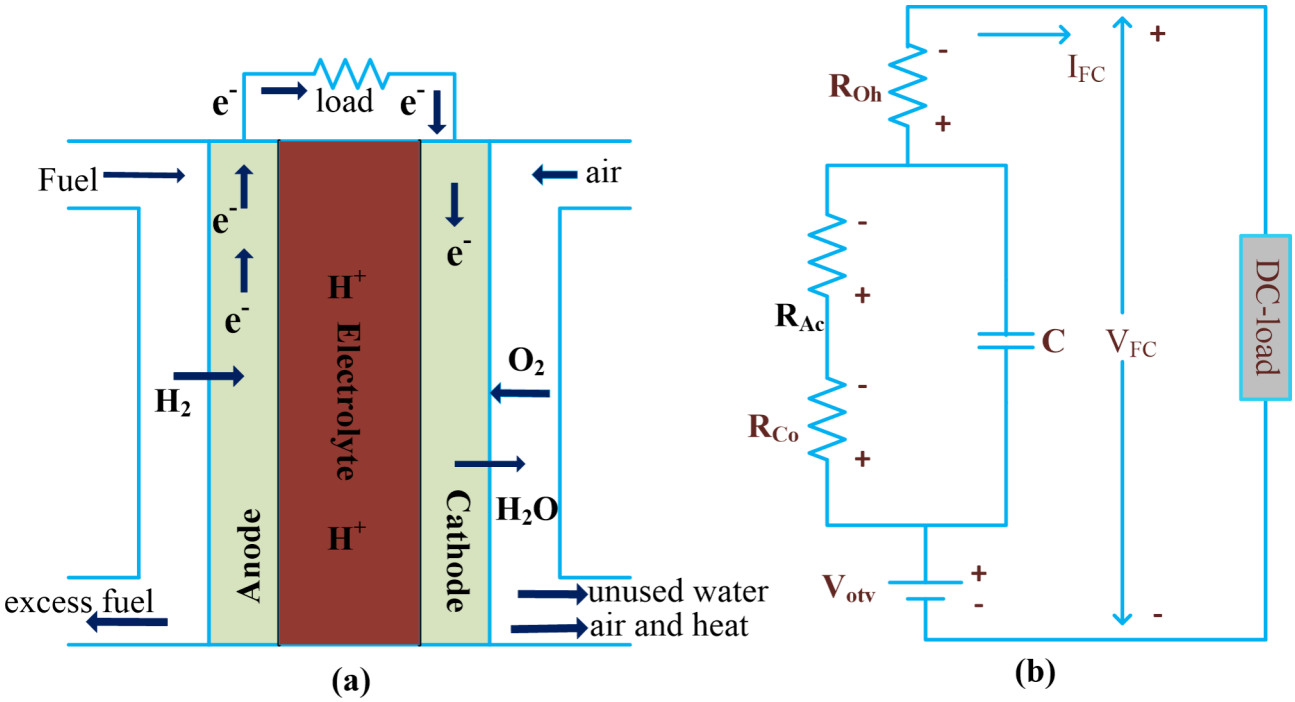

Fig. 3. Utilized polymer membrane electrolyte fuel stack, (a). Chemical reactions, plus (b). Equalized circuit of the fuel stack.

$$P_{O_2} = \frac{1}{2} HV_C * P^{sat}_{H_2O} \left(\frac{1}{\frac{HV_C * P^{sat}_{H_2O}}{P_C} \exp\left(\frac{4.12*(I_{cell}/A)}{1.22*T_{Fop}}\right)} \right) \tag{8}$$

$$V_{Ac} = g_1 + g_2 T_{Fop} + (g_3 + g_4) T_{Fop} \log(C_{O_2} + I_{FC}) \tag{9}$$

$$V_{Co} = -\frac{R*T_{Fop}}{NF} \mathrm{In}\left(1 - \frac{X}{X_{max}}\right) \tag{10}$$

$$V_{Oh} = I_{cell}*(R_{ef} + R_{pf}) \tag{11}$$

$$C_{O_2} = \frac{P_{O_2}}{5.08e^6 * \exp(-498/T_{Fop})} \tag{12}$$

$$X = \frac{I_{cell}}{A} \tag{13}$$

$$R_{ef} = \frac{\gamma_{ef} Q}{A} \tag{14}$$

$$\gamma_{ef} = \frac{181.6 \left[1 + 0.01X + 0.52*(T_{Fop}/303)^2 * X^{2.5}\right]}{(W - 0.634 - 3X)\exp\left(\frac{4.02(T_{Fop} - 304)}{T_{Fop}}\right)} \tag{15}$$

Where T_{Fop}, P_{H2}, and P_{O2} are indicated as operating fuel stack temperature, hydrogen partial pressure, plus oxygen partial pressure. The terms HV_A, HV_c, P_A, P_C, plus P_{H2O} are represented as anode humidity vapor, relative humidity vapor at the cathode, anode partial pressure, cathode partial pressure, plus water pressure of the fuel stack. Here, the empirical coefficients are indicated as g_1, g_2, g_3 plus g_4. Finally, the parameters I_{FC}, F, X, and A are each cell current, faraday constant, overall stack current, and fuel stack chamber area. In the diffusion layer, the oxygen concentration is determined by using Eq. (12). From Eq. (15), the effective resistance of the single cell, and the overall resistance of the fuel stack are represented as r_{ef}, plus R_{ef}. The PEMFS design parameters are given in Table 1, and also the proposed fuel stack power versus current nonlinear characteristics are shown in Fig. 4.

Design, and investigation of controllers

Due to the nonlinear characteristics of the fuel stack, the maximum power extraction from the source is very difficult. So, the MPPT technology plays an important role in tracking the fuel stack MPP position at different water membranes, and operating temperature conditions[52]. Also, from section "Introduction", it is

Parameters	Values
Rated power of the PEMFS	1.26 k Watts
Maximum output voltage of the PEMFS	24.23 Volts
Maximum output current of the PEMFS	52 A
Nominal air flow rate (lpm)	2400
Maximum airflow rate	4615
Number of fuel cells used (N)	42
Nominal supply pressure of H_2	1.5 bar
Nominal supply pressure of O_2	1 bar
Constant of gas (R)	82.899 [J.mol^{-1}.K^{-1}]
Constant of faraday (F)	97,000.912 [C.mol^{-1}]
Oxidant composition	21%
Fuel composition	99.95%
Hydrogen utilization	99.56%
Utilization of oxygen	59.3%
Nerst voltage of each cell (V_{FC})	1.115 V

Table 1. Detailed design parameters of the proton exchange membrane fuel stack.

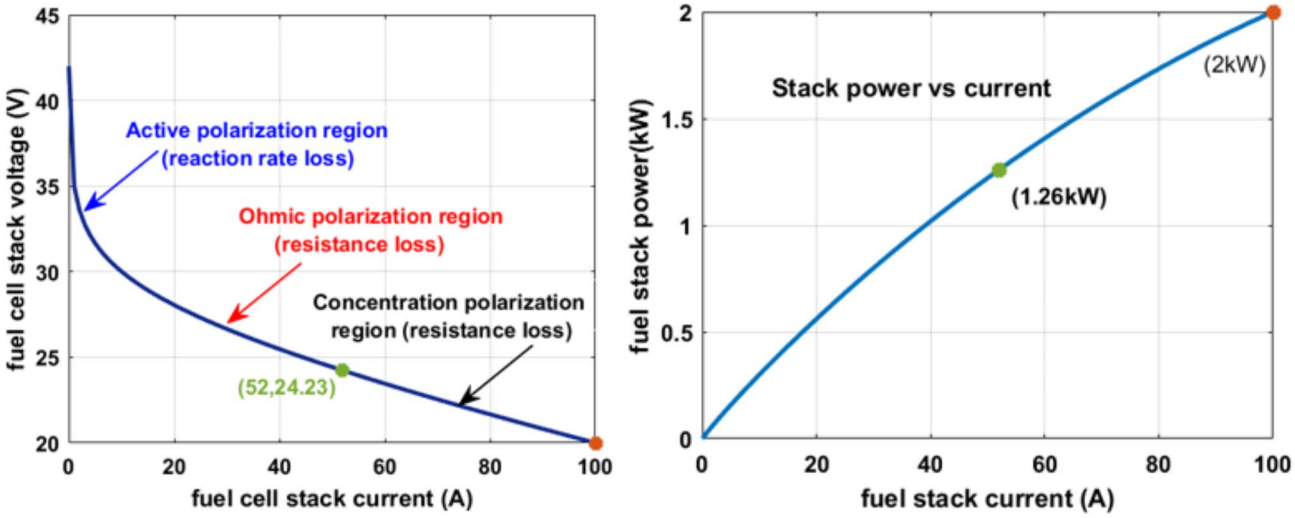

Fig. 4. **(a)** Fuel stack generated V–I curve. **(b).** Fuel stack generated P–I curve.

identified that the general power point tracing methodologies are not suitable for rapid changes in operating temperature conditions of the fuel stack. The conventional MPPT controllers' disadvantages are high output voltage fluctuations, more time for extracting the maximum output voltage, high convergence time, plus needed a greater number of sensing devices. The limitations of conventional controllers are overcome by using the advanced MPPT controllers which are ASV with P&O[53], ASS with IC[54], RBFN[55], IS with FLC[56], CSV with PSO[57], and ASV with CSA.

Adjusted step value-based P&O MPPT technique

As we know the general P&O method is useful only for constant operating temperature conditions of the fuel stack, and it is applied where the accuracy of MPPT is not necessary. This controller's disadvantages are high oscillations across MPP, high power conduction losses, less life span of the system, plus less efficiency. Also, this controller depends on the initial working conditions of the PEMFS[58]. In article[59], the authors focused on the ASV-P&O method which is implemented by using the different steps which are system modeling, power loop control, step constant variation, performance evaluation, and stability. In the system modeling step, the PEMFC characteristics are studied. In the second step, the power loop control continuously adjusts the overall system impedance to track the fuel stack MPP. Here, the PEMFS voltage is perturbated to enhance the power rating of the fuel stack. The advantages of the adjusted step value-based P&O MPPT technique are moderate oscillations across MPP, fast system response, plus high efficiency when equated to the conventional P&O controller[60]. Based on Eq. (16), when the functioning point of the fuel stack is lying on the last corner of the P–I curve then the duty value of the DC-DC converter is improved to move the operating point of the fuel stack near to the actual MPP position. Otherwise, the duty cycle of the converter is reduced which is given in Eq. (17).

$$\delta\ (t) = \delta\ (t-1) + \alpha \left(\frac{p\,(t) - p(t-1)}{v\,(t) - v(t-1)}\right) \tag{16}$$

$$\delta\ (t) = \delta\ (t-1) - \alpha \left(\frac{p\,(t) - p(t-1)}{v\,(t) - v(t-1)}\right) \tag{17}$$

Where the parameters $\delta\ (t)$, and $\delta\ (t-1)$ are the instant duty cycle, plus the previous duty cycle. Here 'α' is an adjustable constant parameter that is used to adjust the duty value. Similarly, the parameters v(t), p(t), v(t–1) & p(t–1) are the present and previous voltages and powers of the fuel stack.

Adaptive step size with incremental conductance

One of the most commonly used conventional MPPT controllers is IC which is applied in traffic signal control systems. The IC concept implementation has been done by utilizing the nonlinear V-I characteristics of the fuel stack. Here, the system conductance is varied continuously until the functioning point of the fuel stack reaches the actual MPP position[61]. In article[62], the adjusted step value-based IC controller is used in the electric vehicle-fed fuel stack system for running slip ring induction machines under continuous changes of water membrane content of the fuel stack. Here, the water electrolysis concept is used for supplying H_2 to the fuel cell banks, and the fuel stack electrodes are designed using copper materials. In this ASS-IC controller, the equivalent impedance of the fuel stack is used for identifying the optimum duty value of the interleaved DC–DC converter. The adjustment of the converter duty cycle by using this MPPT controller is given in Eq. (18), and Eq. (19)[63].

$$\Psi\,(t) = \Psi\,(t-1) + k^* \left(\frac{P\,(t) - P(t-1)}{V\,(t) - V(t-1)}\right) \tag{18}$$

$$\Psi\,(t) = \Psi\,(t-1) - k^* \left(\frac{P\,(t) - P(t-1)}{V\,(t) - V(t-1)}\right) \tag{19}$$

Where the terms $\Psi\,(t)\ \&\ \Psi(t-1)$ is the present duty value, and past duty cycle parameters and their related power changes are represented as p(t), and p(t-1). Finally, the evaluated fuel stack past and instant voltages are v(t−1), and v(t).

Radial basis functional network-based MPPT controller

Mostly, the ANN is used in nonlinear decision-making problems applications[64]. These networks are implemented from the inspiration of biological neurons, and the ANN is designed from the combination of activation functions, mathematical operations, and optimization methodologies. In the article[65], the RBFN model neural controller is interfaced in the automotive fuel stack system to improve the dynamic behavior of EVs[66]. The RBF networks have the capability of approximation of complex functions, good modeling of nonlinear relationships, plus capturing the complex patterns from the available data to determine the accurate MPP position of the fuel stack. The RBF-related power point identifying the network working nature is illustrated in Fig. 5. Based on Fig. 5, the radial function is used as an activation function for obtaining the desirable duty to the DC–DC converter circuit. The RBF demonstrates the smooth transition from the center point to the surroundings of the neurons to adapt to the source space very efficiently. Based on available data sets, the RBF interpolates the input-output relations, and it generalizes the input-output relations for non-available data. The major advantage of RBF is its high computational efficiency.

$$net_T^{(1)} = S_T^1\,(x)\,; x = 1,2,3,4,\ldots,n \tag{20}$$

$$H_L^{(1)}\,(x) = f_T^{(1)}\left(net_T^{(1)}\,(x)\right) = net_T^1\,(x)\,;\ T = 1,2,3 \tag{21}$$

$$net_Y^{(2)}\,(x) = -(S - \mu_Y)^T * \sum\nolimits_Y (S - \mu_Y) \tag{22}$$

$$H_Y^{(2)}\,(x) = f_Y^{(2)}\left(net_Y^{(2)}\left(x\right)\right); Y = 1,2,3,4,\ldots.,9 \tag{23}$$

$$\mu_Y = \left[\ \mu_{1Y}\quad \mu_{2Y}\quad \mu_{3Y}\quad \cdots\cdots\quad \mu_{TY}\ \right] \tag{24}$$

$$\sum\nolimits_Y = \mathrm{diag}\left[\ {}^{1}\!/_{?_{1Y}^2}\quad {}^{1}\!/_{?_{2Y}^2}\quad {}^{1}\!/_{?_{3Y}^2}\quad \cdots\cdots\quad {}^{1}\!/_{\sigma_{LM}^2}\ \right] \tag{25}$$

$$net_U^{(3)} = \sum\nolimits_U W_Y H_Y^2\,(x)\,; x = 1,2,3,4,5,\ldots.,n \tag{26}$$

$$O_U^{(3)}\,(x) = f_U^{(3)}\,((\,net_U^3\,(x)) = net_U^3(x) \tag{27}$$

Where the terms T, U, and Y are the first layer, output layer, plus middle layers. The variables $S_T^1\,(x)\,, net_T^{(1)}\,(x)$ represents the net value of the source layer, and its corresponding output signal. The total selected data samples are identified as 'x'. The $H_L^{(1)}\,(x)$, $H_Y^{(2)}\,(x)$ gives the center layer the first, and second node overall input signal. The hidden layer output net value is determined as $net_Y^{(2)}\,(x)$. The variables 'S', μ , $?, W,$ and O are indicated

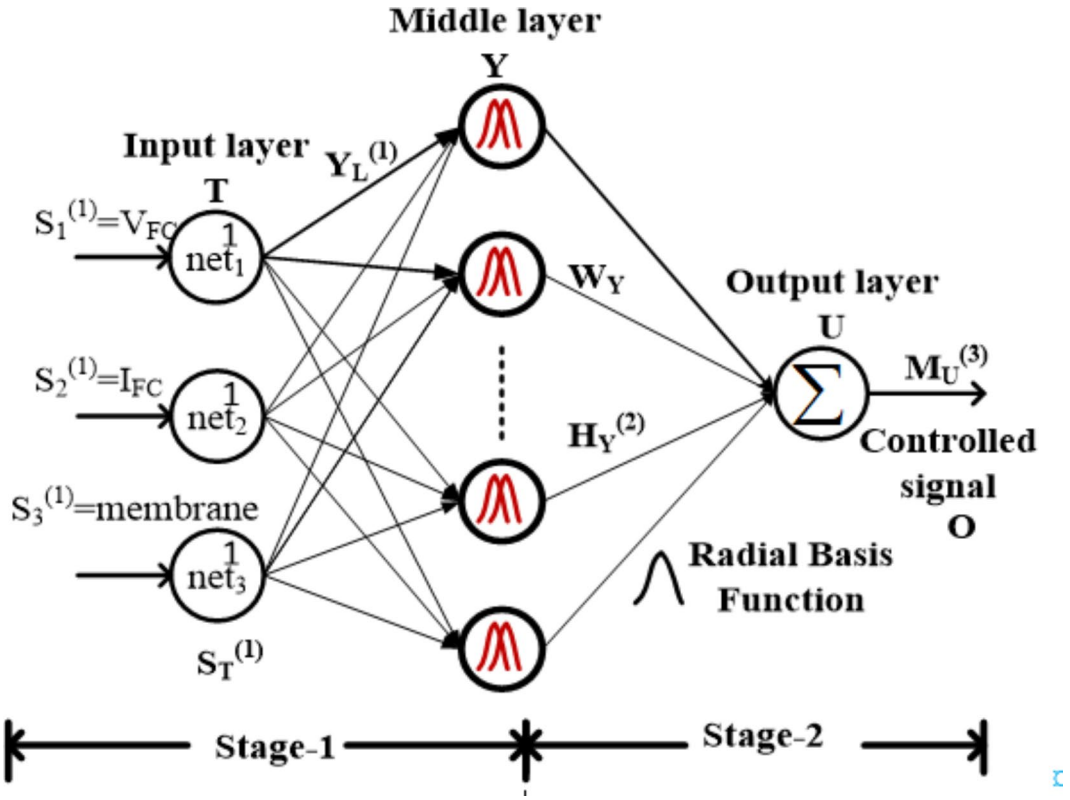

Fig. 5. RBFN work process for PEMFC-based power supply system.

as input vectors, the mean value of the signal, controller coefficient, neuron weight, and required RBF output signal.

Incremental step-fuzzy logic controller

The radial functions have certain drawbacks which are high training complexity. Especially, the training of large data sets and multidimensional input parameters is very difficult. The overfitting problem occurs in RBF networks due to the number of radial basis functions. Selection of suitable radial basis functions is a challenging task for the greater number of radial functions. In the article[67], the fuzzy controller is integrated into the Z-circuit converter-fed fuel stack system to enable the peak power supply of PEMFC at diverse water membranes, and operating temperature conditions[68]. The fuzzy is formed from the mathematical framework which especially deals the impression and uncertainty. Also, the fuzzy handles the linguistic variables and terms to allow the experts to represent their expertise naturally. The fuzzy systems are easily adapted for various multidimensional problems. The features of fuzzy are high flexibility, best suitable for dynamic environmental conditions, and high robustness for handling noisy, and incomplete data[69]. Also, this system works inherently for uncertainty issues, and it consists of more transparency, plus provides high interpretability.

In a fuzzy MPPT block, there are different blocks integrated which are fuzzification of input parameters, execution of various rules of the controller, plus defuzzification of output variables to crisp value for finding the error parameter of the system[70]. The fuzzy controller for the MPPT application is given in Fig. 6, and its rules and membership functions are stated in Fig. 6. The error variables of fuzzy are given in Eq. (28). From Fig. 6, the fuzzy adapts the continuous variation of EV fed fuel stack temperature, and it traces the functioning point of PEMFC on P-I curve with high convergence speed. Here, the fuzzy membership functions are chosen based on the application of optimization techniques. The fuzzy does not involve any mathematical formulas[71]. So, the entire controller implementing cost, and size are reduced. The efficiency of fuzzy MPPT is high when equalized with the neural network because of the multiple-step value selection on the V–I curve. The fuzzy enhances the duty of the converter because the working point of PEMFC is the right-side corner of the actual MPP or else, the duty is varied in a descending fashion to reduce the fluctuations of load power.

$$e(n) = \frac{P(n) - P(n-1)}{V(n) - V(n-1)}\,;\ \Delta e(n) = e(n) - e(n-1) \tag{28}$$

Continuous step variation-based PSO MPPT controller

Sometimes, fuzzy systems are more complex because they need more rules and membership functions. So, the entire controller design, plus maintenance cost is increased[72]. In a hybrid fuel stack/PV power supply, the PSO controller is applied for the continuous improvement of the efficiency of the converter. PSO is one of the

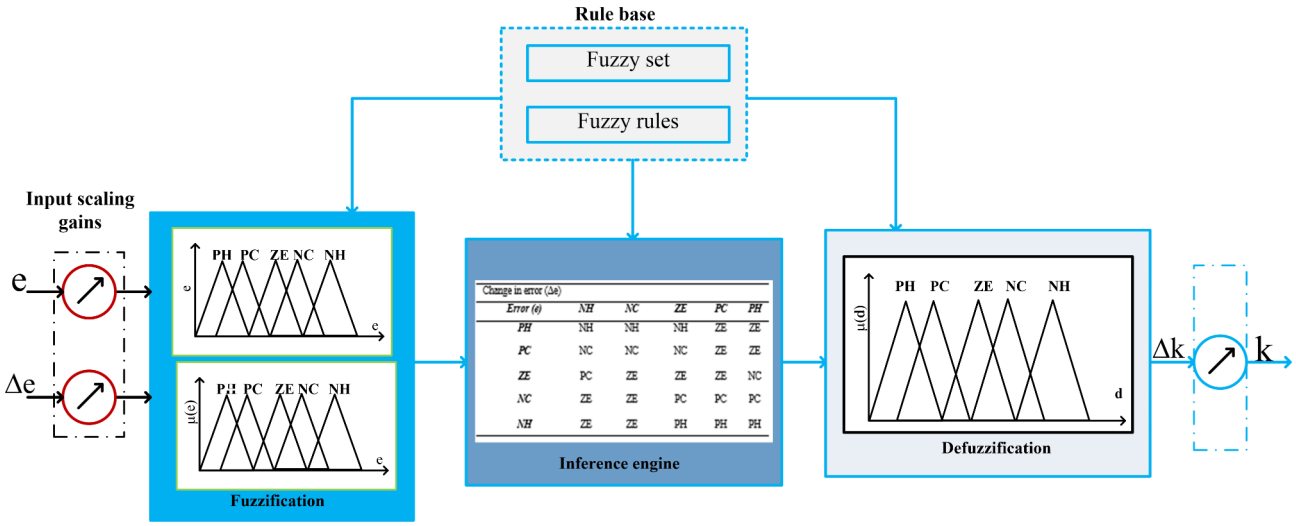

Fig. 6. Improved fuzzy MPPT for fuel stack application.

metaheuristic swarm controllers that can be used for solving any nonlinear issue of the fuel stack[73]. Also, all the fuel stacks are highly complex, plus nonlinear systems. The fuel cells involve many conflicting requirements which are minimum fuel usage, maximizing the available power, plus optimizing the environmental emissions. The PSO handles the multiple objectives of PEMFS at continuous changes in the working temperature of the fuel stack. In the initial stage of PSO, all the swarm agents' weights are given by applying the random probability technique. Here, all the agents work cooperatively, and a single agent is represented as one particle[74].

At the first iteration of PSO, all the agents move away from the required object in various directions with different velocities. After completing certain iterations, the agents try to come near the required target position. In the search process, all the agents exchange their information to extract the peak voltage of the fuel stack[75]. The agent's successive velocity (V), and its associated position (y) are varied based on Eq. (29), plus (30). The MPPT tracking process using PSO is given in Fig. 7.

$$V^{s+1} = W^{*}V_k^s + L_1 g_1 \left(P_{b\_k} - Y_k^s\right) + L_2 g_2 \left(G_{b\_k} - Y_k^s\right) \tag{29}$$

$$Y^{s+1} = Y_k^s + V_k^{s+1} \tag{30}$$

Where, the variables V^{s+1}, and Y^{s+1} are adjusted velocities, plus the position of agents. The terms 's', 'k', P_{b_k}, and G_{b_k} have selected iterations, particle number, each iteration's best global position, and the global position of MPP after completing all the iterations[76]. The constraints L_1, and L_2 are acceleration factors. Similarly, the variables g_1, and g_2 are particle random values.

Adaptive step value-cuckoo search algorithm

One of the known metaheuristics' optimization methods is cuckoo search controllers which are implemented from the breeding nature of cuckoos[77]. This algorithm solves all types of optimization issues, especially in global optimization where the search space is very high. In this technique, there are three conditions involved which are in the initial iteration each cuckoo should give one egg after that in the second condition, all available eggs have more quality then the controller moves to the next condition or else it goes into the previous condition[78]. The algorithm starts initializing the all-cuckoos weights randomly in the overall search space. Each egg gives a solution for the particular optimization issue. Here, each cuckoo egg is identified by applying the fitness function. The main objective of the fitness function is identifying good quality cuckoo eggs. Another major parameter of CS MPPT is levy flight which is incorporated for initializing the random walk of cuckoos[79]. Also, the levy is useful for the deciding step value of the cuckoos in the multidimensional search region. After applying levy flights, there are a few cuckoos laying their eggs in the host nest[80].

The CS controller selects the best solution from the available solution. A good solution for cuckoos is to have the chance to go to the next iteration[81]. To eliminate the overcrowding of nests, the diversity of the population is continued, and some of the worst solutions are removed from the search space for achieving potentially good solutions. The application of adaptive CS MPPT for the fuel stack system is illustrated in Fig. 8. From Fig. 8, the voltage supplying of the fuel stack, and power of the converter circuit are determined at the initial stage of the adaptive CS MPPT controller. Later, the cuckoos start searching for the required object of the system with the speed (V)[82]. The continuous updating of solutions has been done by applying multiple iterations, and various levy flights. The levy limits of the CS technique are derived in Eq. (31). The parameters §, s, q, X, plus Y are represented as operating constant, number iterations, cuckoo length, and distribution curves. Also, parameters a, and b are the levy flight sizes[83].

$$\text{Levy } (\S) = \text{Length}^{-\S} \; ; \; 1.5 < \S < 3.5 \tag{31}$$

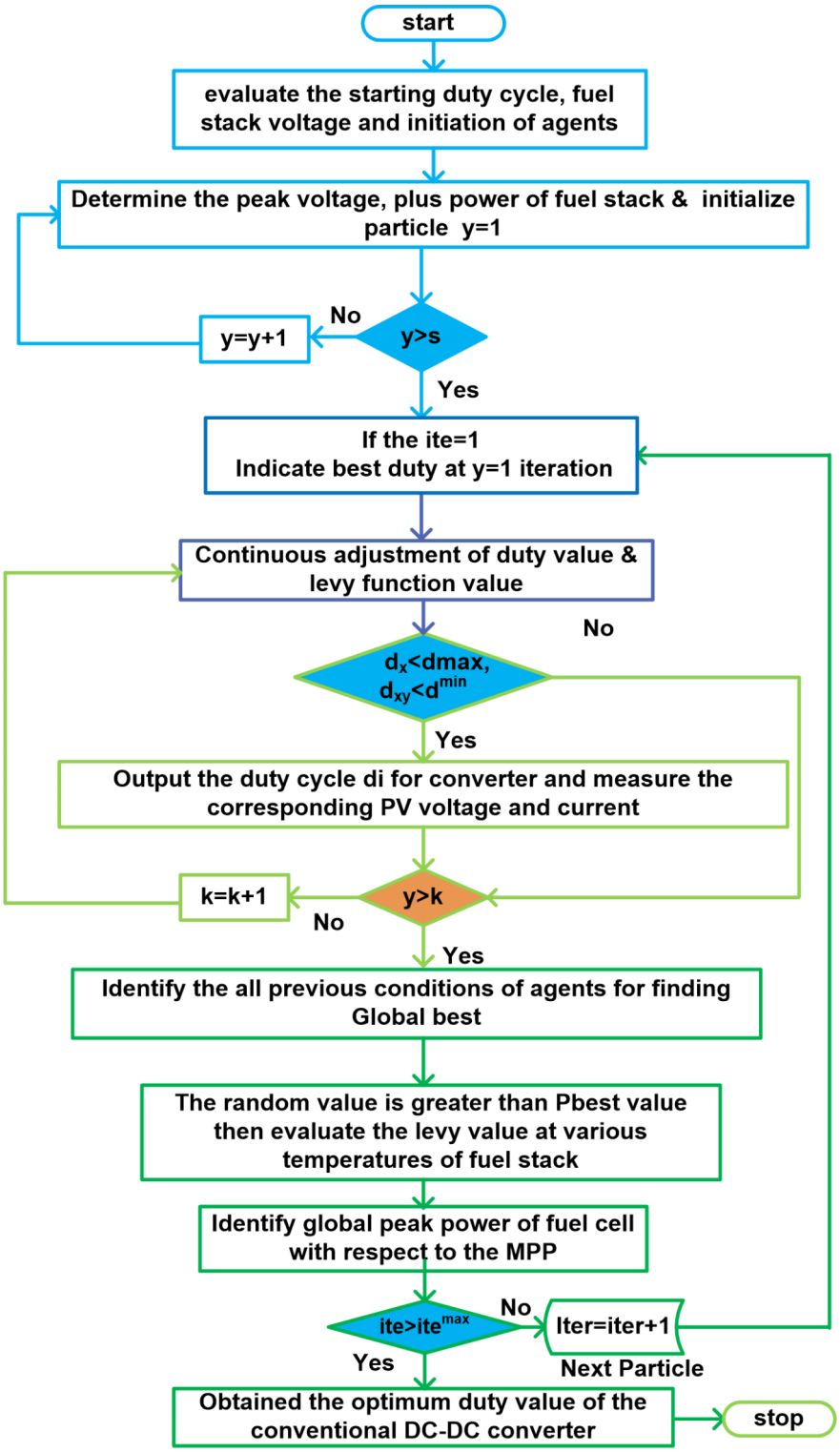

Fig. 7. Continuous step value adjustment of PSO controller for PEMFC system.

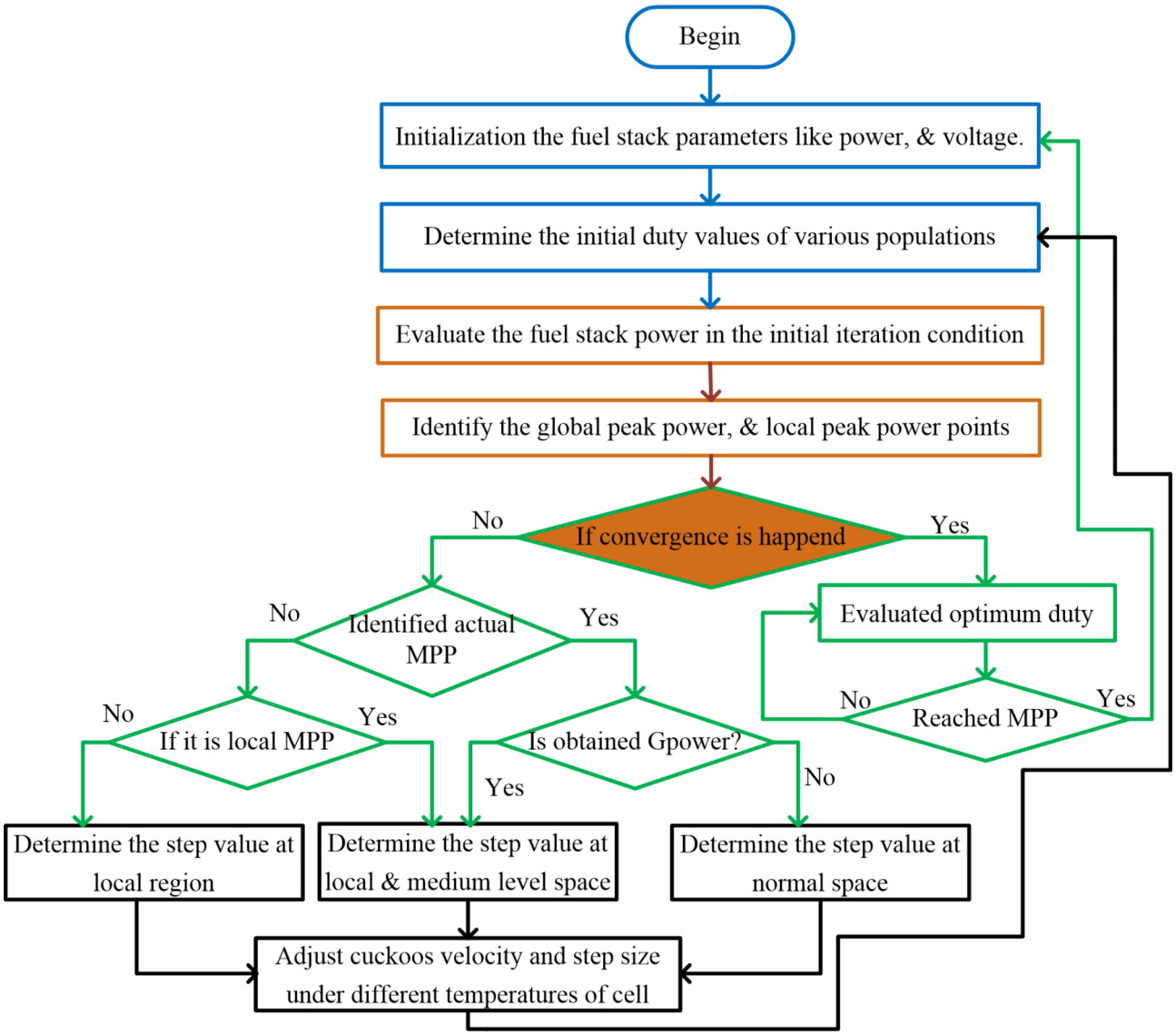

Fig. 8. Improved adaptive CS controller for rapid change of fuel stack temperature.

$$q_j^{s+1} = q_j^s + \alpha \oplus \text{levy}(\S) \tag{32}$$

$$l = \alpha_0 \left(q_{best} - q_j\right) \oplus \text{levy}(\S) \approx c \left(\frac{u}{v^{1/\S}}\right) * \left(q_{best} - q_j\right) \tag{33}$$

$$X = a\left(0,\ \rho_u^2\right), \quad Y = b\left(0,\ \rho_v^2\right) \tag{34}$$

Design of conventional boost DC–DC converter

All the fuel stacks supply very low voltages. So, the output of PEMFC is enhanced by interfacing the DC–DC converter. From the previously existing articles, the isolated converter circuits needed high design costs[84]. Also, these converters need more additional components which are transformers, and rectifier circuits. Due to the additional requirement of the converter, the entire fuel cell power system size is increased. This is undesirable for electric vehicle-fed fuel stacks. So, the conventional non-isolated converter circuit is integrated with the fuel cell to enhance the working efficiency of PEMFC[85]. The general boost converter circuit is frequently used in many applications because of its advantages are easy to design, more flexibility, fewer components required for implementation, optimal size, plus easy understanding and operation. The working stages of this converter circuit are given in Fig. 9(a), (b), and (c)[86]. The step-up of fuel cell voltage is obtained by the application of the MPPT controller which is mentioned in Eq. (35). From Fig. 9, the consumer load current is given in Eq. (36).

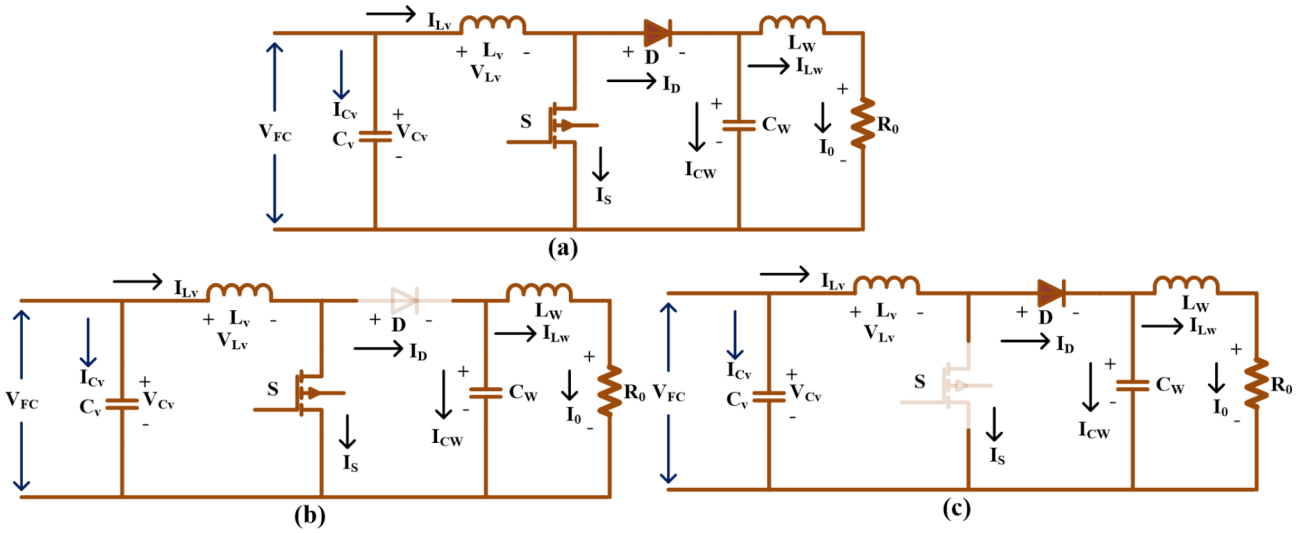

Fig. 9. DC–DC Converter circuit, (a). block diagram, (b). switch working, plus (c). switch blocking stage.

Based on Eqs. (35), and (36), the current plus voltage conversion ratios are determined which are given in Eq. (37).

$$DT_p{*}V_{FC} + (1-D)\,T_p{*}\,(V_{FC} - V_0) = 0 \tag{35}$$

$$-I_0 D{*}T_P + ((I_{FC} - I_0){*}\,(1-D)\,T_p = 0 \tag{36}$$

$$V_0 = {}^{V_{FC}}\!/_{(1-D)} \;\&,\; I_0 = I_{FC}\,(1-D) \tag{37}$$

Where T_p, and D are the switching period and converter duty value. Similarly, the terms I_0, plus V_0 are the load currents and voltages.

Analysis of summation results

The resistive load boost converter circuit is integrated with the PEMFC to improve the power supply capacity of the load with less power conduction losses. The entire system investigation has been done by the use of the MATLAB Simulink tool. Here, the polymer-type fuel stack is selected for the power supply of peak load demand. This fuel stack takes hydrogen, and water for the production of electrons. The selected rated power of the stack is $1.26{*}10^3$ W, and its supply voltage is 24.23 V. The current flow through the circuit is 52 A which can be optimized by using the DC–DC converter. The fuel stack output capacitor value C_v is 38 µF that is maintained constant supply voltage under rapid changes in fuel stack temperatures. Also, this capacitor optimizes the ripples of fuel stack power thereby enhancing the performance of the entire power supply system. The load capacitor C_w value is 23 µF, and it is helpful for the consumer to maintain the uninterruptable load voltage.

Analysis of MPPT controllers at static 270 K temperature

Here, under the forward stage of a switch, the diode goes into the blocking stage, and the entire supply energy is stored in the inductor L_V. In the second stage, the switch (S) goes off-stage then the diode conducts with supply voltage. Here, the MOSFET is selected for analysis of the DC–DC converter circuit. The features of this device are high input resistance, the switch works very fast manner, less power absorption, plus less output resistance. Also, this device works in both depletion and enrichment mode operations. The ASV with P&O and ASS with IC controllers fed fuel stack system give the maximum power, plus currents are 362.84 W, 24.5 A, 451.98 W, plus 27 A respectively. The obtained current, plus the voltage of the PEMFC system are explained in Fig. 10(a), and (b). The evaluated fuel stack power by interfacing the RBFN, IS with FLC, plus CSV with PSO is 494.13 W, 531.88 W, plus 555.80 W as given in Fig. 10(c). From Fig. 10(c), the resistive load connected to ASV with the CSA controller extracts more power from the PEMFC which is equal to 567.82 W. The supply voltage of PEMFC is increased by the application of CSV with PSO, and ASV with CSA controller. The DC-DC converter circuit is fed to the load and its related voltage, plus powers by the application of ASV with P&O, ASS with IC, RBFN, IS with FLC, CSV with PSO, plus ASV with CSA techniques are 108.5 V, 294.25 W, 118.07 V, 349.48 W, 123.05 V, 375.42 W, 127.21 V, 400.717 W, 128.004 V, 409.86 W, 128.93 V, plus 416.18 W. The application of MPPT controllers for the converter current and voltage improvement is given in Fig. 10(d), and (e). From Fig. 10(f), the generated converter power by utilizing ASV with CS is very high when equated to the ASV with P&O, RBFN, and IS with FLC techniques. The converter voltage and PEMFC system MPP oscillations are more for the application of ASV with a P&O controller. The evaluated parameters of various MPPT controllers for the DC–DC converter circuit fed fuel stack system are given in Table 2.

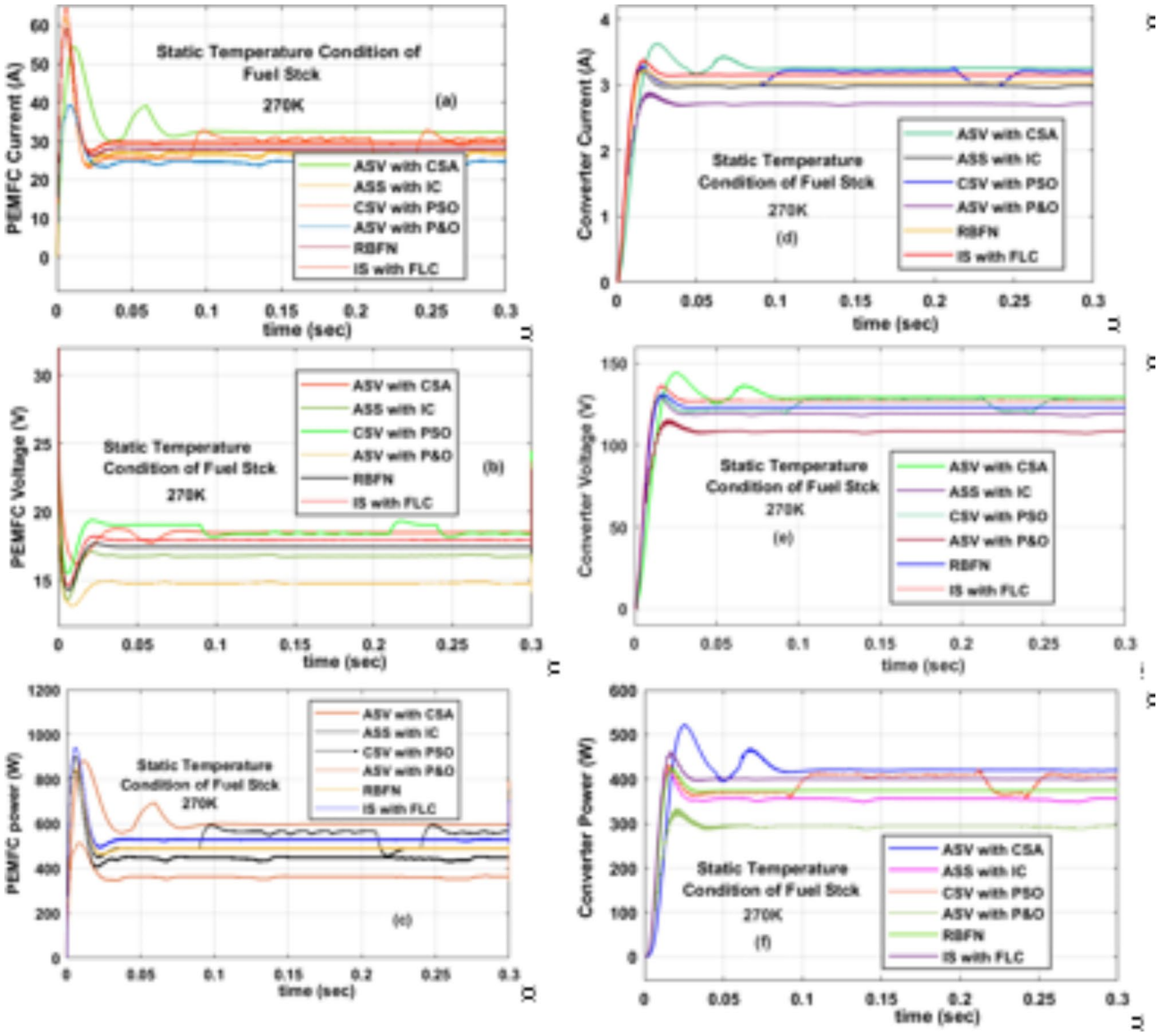

Fig. 10. PEMFC, (a). Current, (b). Voltage, (c). Power, (d). DC–DC current, (e). DC–DC voltage, and (f). DC–DC power under the static functioning temperature of the fuel stack.

Analysis of MPPT controllers at dynamic temperatures (270 K, 300 K, and 330 K)

The PEMFC system is studied at fast changes in temperature values by the integration of different MPPT blocks. The fuel stack MPP tracking speed by the use of ASV with P&O, ASS with IC, RBFN, IS with FLC, CSV with PSO, plus ASV with CSA controllers at 270 K are 0.081 s, 0.102 s, 0.11 s, 0.127 s, 0.1281 s, plus 0.1288 s. The conventional ASS with IC, plus ASV with P&O controllers' implementation, and design complexity is quite less than the other power point identifying controllers. At 300 K, the fuel stack, and DC-DC converter circuit available currents, and voltages by applying the CSV with PSO, and ASV with CSA are 37.29 A, 22.8 V, 4.02 A, 152.79 V, 38.09 A, 22.98 V, 4.089 A, plus 153.98 V respectively. At dynamic temperature states of the fuel stack, the supply current, plus voltage waveforms of the PEMFC system are illustrated in Fig. 11(a), and (b). There are multiple types of power point determine controllers utilized for the improvement of the output power of PEMFC under dynamic functioning temperatures as given in Fig. 11(c).

Based on Fig. 11(c), the settling time of fuel power is high for the application of ASV with the P&O technique. Also, this ASV with P&O methodology is not useful for supplying the constant current to the load as mentioned in Fig. 11(d). The converter generated voltage and its related powers are mentioned in Fig. 11(e), and (f). From the converter circuit, current waveforms at 330 K by utilizing the ASV with CSA, and CSV with PSO consist of fewer distortions. Also, their tracking speeds under static as well as fast variations of fuel stack functioning temperatures are high which are evaluated as 0.1273 s, and 0.1277 s respectively. Here, the swarm optimization methodologies' design complexity is moderate. However, these techniques are needed for optimizing the oscillations of fuel stack voltages thereby minimizing the working power and heating losses are decreased

MPPT type	Cell current (A)	Cell voltage (V)	Cell power (W)	Converter current (A)	Converter voltage (V)	Converter power (W)	Efficiency of MPPT (%)	Tracking speed (s)	Oscillations of MPP	Complexity in design
The converter-fed fuel stack running temperature is 270 K										
ASV with P&O	24.5	14.81	362.84	2.712	108.50	294.25	97.66	0.081	More	Less
ASS with IC	27.0	16.74	451.98	2.960	118.07	349.48	97.69	0.102	More	Less
RBFN	28.22	17.51	494.13	3.051	123.05	375.42	97.78	0.110	Medium	Medium
IS with FLC	29.5	18.03	531.88	3.150	127.212	400.717	97.83	0.127	Medium	Medium
CSV with PSO	29.58	18.79	555.80	3.202	128.004	409.86	97.88	0.1281	Less	Medium
ASV with CSA	29.65	19.151	567.82	3.228	128.93	416.18	97.91	0.1288	Less	Medium
The converter-fed fuel stack running temperature is 300 K										
ASV with P&O	34.01	20.22	687.68	3.71	145.66	540.39	97.74	0.08	More	Less
ASS with IC	34.19	21.19	724.48	3.78	147.80	558.68	97.79	0.092	More	Less
RBFN	35.35	22.20	784.77	3.842	148.17	569.26	97.81	0.1262	Medium	Medium
IS with FLC	36.89	22.69	837.03	3.97	151.55	601.65	97.98	0.1275	Medium	Medium
CSV with PSO	37.29	22.8	856.92	4.02	152.79	614.21	98.00	0.1277	Less	Medium
ASV with CSA	38.09	22.98	875.30	4.089	153.98	629.62	98.74	0.12865	Less	Medium
The converter-fed fuel stack running temperature is 330 K										
ASV with P&O	43.13	25.80	1112.7	4.55	189.99	864.45	97.82	0.079	More	Less
ASS with IC	43.89	25.81	1132.8	4.713	190.78	899.14	97.88	0.091	More	Less
RBFN	44.11	26.89	1186.1	4.79	190.91	914.45	97.92	0.1258	Medium	Medium
IS with FLC	45.29	27.10	1222.8	4.80	191.33	918.38	98.02	0.1271	Medium	Medium
CSV with PSO	45.30	27.25	1234.4	4.872	192.88	939.71	98.22	0.1273	Less	Medium
ASV with CSA	45.33	27.29 V	1237.1	4.932	194.19	957.74	99.90	0.1277	Less	Medium

Table 2. Simulative results analysis of different power point identifying methods under quick variation of fuel stack temperatures.

extensively. The conventional may not give a good dynamic response because of their accuracy in MPP finding and required high maitainence cost.

Conclusion

The proposed PEMFS-fed ASV with a CSA-based MPPT controller is designed by using the MATLAB/Simulink tool. Here, in the first objective, the PEMFS is selected for the comprehensive analysis of different nature-inspired optimization controllers. The features of PEMFS are high-temperature withstand ability, high operating efficiency, less weight, high scalability, plus more life span. However, the drawback of PEMFS is the high output current. In the second objective, the DC–DC converter circuit is used to optimize the fuel stack output current and increase the fuel stack output voltage. However, the converter needed a suitable duty signal which is generated by using the MPPT controller. Finally, in the third objective, there are different types of MPPT controllers are analyzed in terms of maximum power extraction, settling time of the converter output voltage, oscillations across MPP, convergence speed of the MPPT controller, and implementation complexity. From the comprehensive summary, the ASV with CSA-based MPPT controller is giving high tracking speed of MPP, and high efficiency when compared to the other MPPT controllers.

Future scope of the work

The present studied MPPT controllers have the limitations of moderate MPP tracking accuracy, and less convergence speed when the total number of iterations are required very high at continuous changes of operating temperature conditions of the polymer exchange membrane fuel stack. In the future, the nature-inspired PSO, and ASV with CSA-based MPPT controllers' hybridization has been done along with the conventional controller to increase the MPP tracking accuracy and find the optimum duty cycle of the DC–DC converter.

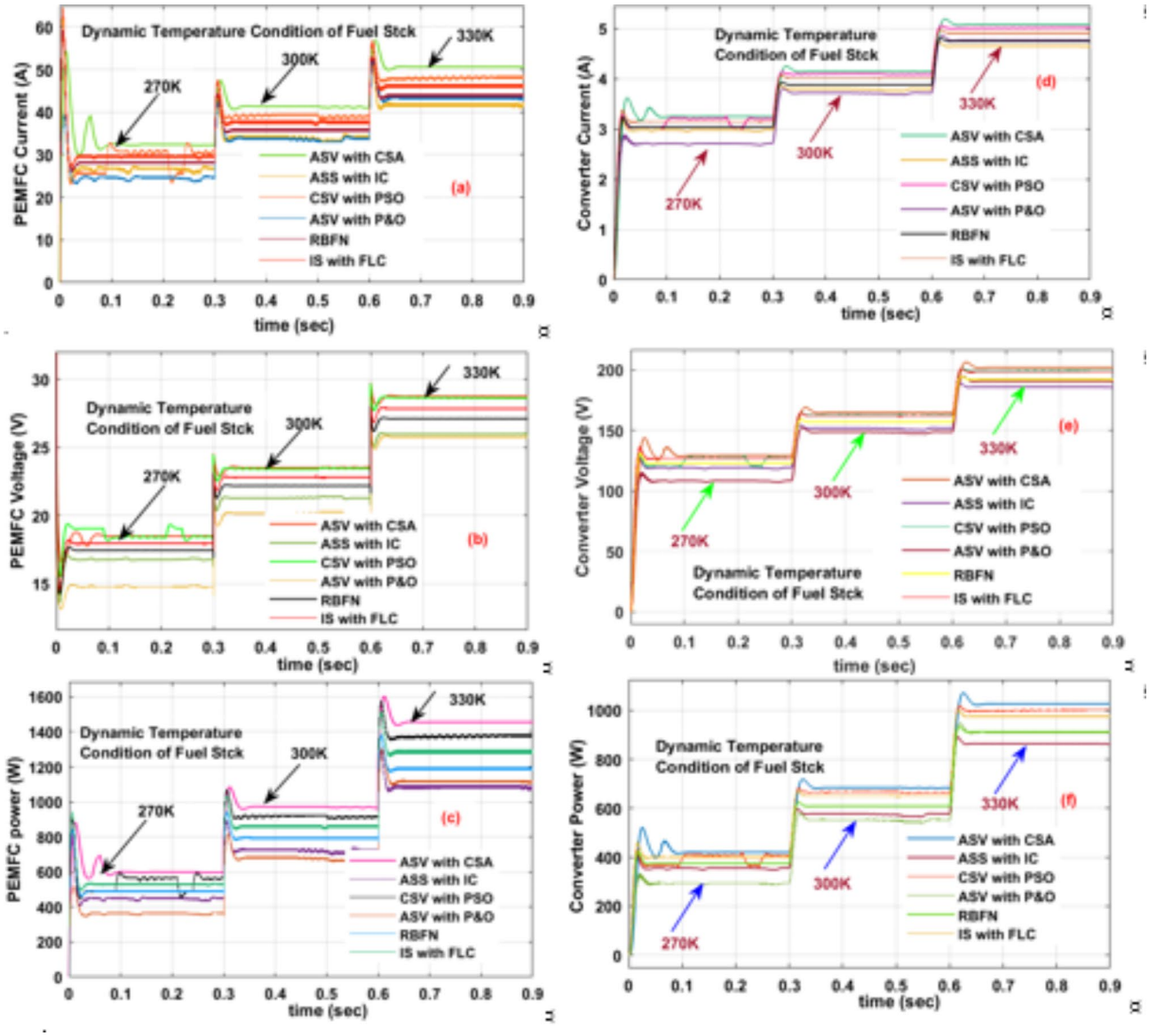

Fig. 11. PEMFC, (a). Current, (b). Voltage, (c). Power, (d). DC–DC current, (e). DC–DC voltage, and (f). DC–DC power under the dynamic functioning temperature of the fuel stack.

Data availability

The datasets used and/or analyzed during the current study are available from the corresponding author upon reasonable request.

Received: 30 July 2024; Accepted: 11 September 2024
Published online: 16 September 2024

References

1. Rather, K., Nesar, M. K., Mahalik & Mallick, H. Do renewable energy sources perfectly displace non-renewable energy sources? Evidence from Asia–Pacific economies. *Environ. Sci. Pollut. Res.* **31**, 25706–25720 (2024).
2. Behera, B. et al. A blend of renewable and non-renewable energy consumption on economic growth of India: the role of disaggregate energy sources. *Environ. Sci. Pollut. Res.* **31**(3), 3902–3916 (2024).
3. Khalid, M. Smart grids and renewable energy systems: perspectives and grid integration challenges. *Energy Strategy Reviews* **51**, 101299 (2024).
4. Benbouhenni, H. et al. A new integral-synergetic controller for direct reactive and active powers control of a dual-rotor wind system. *Meas. Control* **57**(2), 208–224 (2024).
5. Hodel, H. et al. Which wind turbine types are needed in a cost-optimal renewable energy system? *Wind Energy* (2024).
6. Sun, H. et al. Optimal scheduling considering Carbon capture and demand response under Uncertain output scenarios for wind energy. *Sustainability* **16**(3), 970 (2024).

7. Hussaian Basha, C. H. et al. Design and performance analysis of common duty ratio controlled zeta converter with an adaptive P&O MPPT controller. In *Proceedings of International Conference on Data Science and Applications: ICDSA. Volume 1* (Springer, 2022).
8. Fawzy, S. et al. Optimal location and operation of energy storage and transmission switching for minimizing wind power spillage. *J. Energy Storage* **90**, 111925 (2024).
9. Wang, R. et al. FI-NPI: exploring optimal control in parallel platform systems. *Electronics* **13**(7), 1168 (2024).
10. Basha, C. H. H. et al. A novel on intelligent energy control strategy for micro grids with renewables and EVs. *Energy Strategy Rev.* **52**, 101306 (2024).
11. Tian, H. et al. Dynamic analysis and sliding Mode Synchronization Control of Chaotic Systems with conditional symmetric fractional-order memristors. *Fractal Fract.* **8**(6), 307 (2024).
12. Zhang, J. et al. A novel multiple-Medium-AC-Port power electronic transformer. *IEEE Trans. Ind. Electron.* (2023).
13. Zhang, J. et al. An embedded DC power flow controller based on full-bridge modular multilevel converter. *IEEE Trans. Industr. Electron.* **71**(3), 2556–2566 (2023).
14. Fang, S. et al. A novel adaptive fast sliding mode control method based on fuzzy algorithm for the air management system of fuel cell stack. *Process Saf. Environ. Prot.* **187**, 506–517 (2024).
15. Liu, Q. et al. Transfer-free in-situ synthesis of high-performance polybenzimidazole grafted graphene oxide-based Proton exchange membrane for high-temperature proton exchange membrane fuel cells. *J. Power Sourc.* **559**, 232666 (2023).
16. Ju, Y. et al. Distributed three-phase power flow for AC/DC hybrid networked microgrids considering converter limiting constraints. *IEEE Trans. Smart Grid* **13**(3), 1691–1708 (2022).
17. Li, M. et al. Scaling-basis chirplet transform. *IEEE Trans. Ind. Electron.* **68**(9), 8777–8788 (2021).
18. Sun, Q. et al. Virtual current compensation-based quasi-sinusoidal-wave excitation scheme for switched reluctance motor drives. *IEEE Trans. Industr. Electron.* (2023).
19. Shirkhani, M. et al. A review on microgrid decentralized energy/voltage control structures and methods. *Energy Rep.* **10**, 368–380 (2023).
20. Sorlei, I. S. et al. Fuel cell electric vehicles—a brief review of current topologies and energy management strategies. *Energies* **14**(1), 252 (2021).
21. Bizon, N. Sensitivity analysis of the fuel economy strategy based on load-following control of the fuel cell hybrid power system. *Energy. Conv. Manag.* **199**, 111946 (2019).
22. Bizon, N. Real-time optimization strategy for fuel cell hybrid power sources with load-following control of the fuel or air flow. *Energy. Conv. Manag.* **157**, 13–27 (2018).
23. Bizon, N. Fuel saving strategy using real-time switching of the fueling regulators in the proton exchange membrane fuel cell system. *Appl. Energy* **252**, 113449 (2019).
24. Liang, J. et al. A direct yaw moment control framework through robust TS fuzzy approach considering vehicle stability margin. *IEEE/ASME Trans. Mechatron.* **29**(1), 166–178 (2023).
25. Chen, J. et al. Hybrid modeling for vehicle lateral dynamics via AGRU with a dual-attention mechanism under limited data. *Control Eng. Pract.* **151**, 106015 (2024).
26. Yaghoubi, E. et al. A systematic review and meta-analysis of machine learning, deep learning, and ensemble learning approaches in predicting EV charging behavior. *Eng. Appl. Artif. Intell.* **135**, 108789 (2024).
27. Zhou, M. et al. Robust rgb-t tracking via adaptive modality weight correlation filters and cross-modality learning. *ACM Trans. Multimedia Comput. Commun. Appl.* **20**(4), 1–20 (2023).
28. Saidi, S. et al. Precise parameter identification of a PEMFC model using a robust enhanced salp swarm algorithm. *Int. J. Hydrog. Energy* **71**, 937–951 (2024).
29. Basha, C. H., Hussaian & Rani, C. Different conventional and soft computing MPPT techniques for solar PV systems with high step-up boost converters: a comprehensive analysis. *Energies* **13**(2), 371 (2020).
30. Kiran, S. et al. Reduced simulative performance analysis of variable step size ANN based MPPT techniques for partially shaded solar PV systems. *IEEE Access* **10**, 48875–48889 (2022).
31. Pathak, P., Kumar, A. K., Yadav & Alvi, P. A. A state-of-the-art review on shading mitigation techniques in solar photovoltaics via meta-heuristic approach. *Neural Comput. Appl.* **2022**, 1–39. (2022).
32. Pathak, P. et al. Fuel cell-based topologies and multi-input DC–DC power converters for hybrid electric vehicles: a comprehensive review. *IET Gener. Transm. Distrib.* **16**(11), 2111–2139 (2022).
33. Hussaian Basha, C. H. & Rani, C. Performance analysis of MPPT techniques for dynamic irradiation condition of solar PV. *Int. J. Fuzzy Syst.* **22**(8), 2577–2598 (2020).
34. Li, Luoyi, et al. "Seasonal hydrogen energy storage sizing: Two-stage economic-safety optimization for integrated energy systems in northwest China." *iScience* 27.9 (2024).
35. Basha, C. H. & Murali, M. A new design of transformerless, non-isolated, high step-up DC-DC converter with hybrid fuzzy logic MPPT controller. *Int. J. Circuit Theory Appl.* **50**(1), 272–297 (2022).
36. Basha, C., Hussaian & Rani, C. Design and analysis of transformerless, high step-up, boost DC-DC converter with an improved VSS-RBFA based MPPT controller. *Int. Trans. Electr. Energy Syst.* **30**(12), e12633 (2020).
37. Zhu, C. Y. Intelligent robot path planning and navigation based on reinforcement learning and adaptive control. *J. Logist Inf. Serv. Sci.* **10**(3), 235–248 (2023).
38. Yang, Y. et al. Broadband electrical impedance matching of sandwiched piezoelectric ultrasonic transducers for structural health monitoring of the rail in-service. *Sens. Actuat. A: Phys.* **364**, 114819 (2023).
39. Meng, Q. et al. An online reinforcement learning-based energy management strategy for microgrids with centralized control. *IEEE Trans. Ind. Appl.* (2024).
40. Basha, C., Hussaian, C., Rani & Odofin, S. Analysis and comparison of SEPIC, Landsman and Zeta converters for PV fed induction motor drive applications. In *2018 International Conference on Computation of Power, Energy, Information and Communication (ICCPEIC). IEEE* (2018).
41. Meng, Q. et al. *Revolutionizing Photovoltaic Consumption and Electric Vehicle Charging: A Novel Approach for Residential Distribution Systems* (IET Generation, Transmission & Distribution, 2024).
42. Wu, J., Wang, Y. & Yin, C. Curvilinear multilane merging and platooning with bounded control in curved road coordinates. *IEEE Trans. Veh. Technol.* **71**(2), 1237–1252 (2021).
43. Basha, C. H., Hussaian & Rani, C. A new single switch DC-DC converter for PEM fuel cell-based electric vehicle system with an improved beta-fuzzy logic MPPT controller. *Soft. Comput.* **26**(13), 6021–6040 (2022).
44. Zhou, Z. et al. Short-term lateral behavior reasoning for target vehicles considering driver preview characteristic. *IEEE Trans. Intell. Transp. Syst.* **23**(8), 11801–11810 (2021).
45. Li, P. et al. A distributed economic dispatch strategy for power–water networks. *IEEE Trans. Control Netw. Syst.* **9**(1), 356–366 (2021).
46. Nadimuthu, L. P. et al. Energy conservation approach for continuous power quality improvement: a case study. *IEEE Access.* **9**, 146959–146969 (2021).
47. Govinda, C. et al. *Hybrid Fuzzy logic-based MPPT for wind Energy Conversion System. Soft Computing for Problem Solving: SocProS 2018, Volume 2* (Springer, 2020).

48. Huang, Zihao, et al. Performance analysis and multi-objective optimization of a novel solid oxide fuel cell-based poly-generation and condensation dehumidification system. *Energy Conversion and Management* 319 (2024): 118935.
49. Wang, Haowen, et al. A MTPA and flux-weakening curve identification method based on physics-informed network without calibration. *IEEE Transactions on Power Electronics* (2023).
50. Hussaian Basha, C. H. et al. *Simulation of Metaheuristic Intelligence MPPT Techniques for Solar PV Under Partial Shading Condition. Soft Computing for Problem Solving: SocProS. Volume 1* (Springer, 2018).
51. Duan, Y., Zhao, Y. & Jiangping, H. An initialization-free distributed algorithm for dynamic economic dispatch problems in microgrid: modeling, optimization and analysis. *Sustain. Energy Grids Netw.* **34**, 101004 (2023).
52. Lu, Y. et al. Adaptive disturbance observer-based improved super-twisting sliding mode control for electromagnetic direct-drive pump. *Smart Mater. Struct.* **32**(1), 017001 (2022).
53. Xu, B. et al. A novel adaptive filtering for cooperative localization under compass failure and non-gaussian noise. *IEEE Trans. Veh. Technol.* **71**(4), 3737–3749 (2022).
54. Murali, M. et al. Design and analysis of neural network-based MPPT technique for solar power-based electric vehicle application. In *Proceedings of Fourth International Conference on Inventive Material Science Applications: ICIMA 2021* (Springer, 2022).
55. Udhay Sankar, V. et al. *Application of wind-driven Optimization for decision-making in Economic Dispatch Problem. Soft Computing for Problem Solving: SocProS 2018, Volume 1* (Springer, 2020).
56. Basha, C., Hussaian, C., Rani & Odofin, S. Design and switching loss calculation of single leg 3-level 3-phase VSI. 2018 In I*nternational Conference on Computation of Power, Energy, Information and Communication (ICCPEIC)* (IEEE, 2018).
57. Mariprasath, T. et al. Design and analysis of an improved artificial neural network controller for the energy efficiency enhancement of wind power plant. In *Computational Methods and Data Engineering: Proceedings of ICCMDE 2021* 67–77 (Springer Nature, 2022).
58. Kumari, P. et al. Application of DSO algorithm for estimating the parameters of triple diode model-based solar PV system. *Sci. Rep.* **14**(1), 3867 (2024).
59. Li, Luoyi, et al. Multi-dimensional economy-durability optimization method for integrated energy and transportation system of net-zero energy buildings. *IEEE Transactions on Sustainable Energy* 15.1 (2023): 146–159.
60. Pathak, P., Kumar, A. K., Yadav, P. & Ahmad, A. Advanced solar MPPT techniques under uniform and non-uniform irradiance: a comprehensive review. *J. Sol. Energy Eng.* **142**(4), 040801 (2020).
61. Kumbhar, A. et al. Reducing grid dependency and operating cost of micro grids with effective coordination of renewable and electric vehicle's storage. In *Soft Computing for Problem Solving: Proceedings of the SocProS 2022* 639–653 (Springer Nature, 2023).
62. Ibrahim, M. et al. Optimizing step-size of perturb & observe and incremental conductance MPPT techniques using PSO for grid-tied PV system. *IEEE Access.* **11**, 13079–13090 (2023).
63. de Jesús Rubio, J. et al. Energy processes prediction by a convolutional radial basis function network. *Energy* **284**, 128470 (2023).
64. Minh, L. et al. Ensemble models based on radial basis function network for landslide susceptibility mapping. *Environ. Sci. Pollut. Res.* **30**(44), 99380–99398 (2023).
65. Wang, Y. & Fu, L. Study on regional tourism performance evaluation based on the fuzzy analytic hierarchy process and radial basis function neural network. *Ann. Oper. Res.* **2023**, 1–28. (2023).
66. Bai, J. et al. Physics-informed radial basis network (PIRBN): a local approximating neural network for solving nonlinear partial differential equations. *Comput. Methods Appl. Mech. Eng.* **415**, 116290 (2023).
67. Rodríguez-Abreo, O. et al. Fuzzy logic controller for UAV with gains optimized via genetic algorithm. *Heliyon* **10**, 4 (2024).
68. Maroua, B. et al. Robust type 2 fuzzy logic control microgrid-connected photovoltaic system with battery energy storage through multi-functional voltage source inverter using direct power control. *Energy Rep.* **11**, 3117–3134 (2024).
69. Maghfiroh, H., Wahyunggoro, O. & Adha Imam, C. Energy management in hybrid electric and hybrid energy storage system vehicles: a fuzzy logic. *Controll. Rev. IEEE Access.* (2024).
70. Anssari, O. M., Hussein, M., Badamchizadeh & Ghaemi, S. Designing of a PSO-based adaptive SMC with a Multilevel Inverter for MPPT of PV systems under rapidly changing weather conditions. *IEEE Access.* **12**, 41421–41435 (2024).
71. Hussaian Basha, C. H. et al. Design of an adaptive fuzzy logic controller for solar PV application with high step-up DC–DC converter.In *Proceedings of Fourth International Conference on Inventive Material Science Applications: ICIMA 2021*. (Springer, 2022).
72. Ofoli, A. R. *Fuzzy-logic Applications in Electric Drives and Power Electronics. Power Electronics Handbook* 1233–1260 (Butterworth-Heinemann, 2024).
73. Mariprasath, T. et al. A novel on high voltage gain boost converter with cuckoo search optimization based MPPTController for solar PV system. *Sci. Rep.* **14** (1), 8545 (2024).
74. Touti, E. et al. A Novel Design and Analysis Adaptive Hybrid ANFIS MPPT Controller for PEMFC-Fed EV Systems. *Int. Trans. Electr. Energy Syst.* **1**(2024): 5541124 (2024).
75. Águila-León, J. et al. Optimizing photovoltaic systems: a meta-optimization approach with GWO-Enhanced PSO algorithm for improving MPPT controllers. *Renew. Energy* **230**, 120892 (2024).
76. Xu, Bo, and Yu Guo. A novel DVL calibration method based on robust invariant extended Kalman filter." *IEEE Transactions on Vehicular Technology* 71.9 (2022): 9422–9434.
77. Regaya, C. et al. Real-time implementation of a novel MPPT control based on the improved PSO algorithm using an adaptive factor selection strategy for photovoltaic systems. *ISA Trans.* **146**, 496–510 (2024).
78. Ahmed, W., Manohar, P. & Hussaian Basha, C. H. A novel transient analysis of multiterminal VSC-HVDC system incorporating superconducting fault current limiter. *Int. Trans. Electr. Energy Syst.* **1**(2024): 5549066 (2024).
79. Dennai, M., Yassine, H., Tedjini & Nasri, A. Comparative assessment of P&O, PSO sliding mode, and PSO-ANFIS controller MPPT for microgrid dynamics. *Elektronika Ir. Elektrotechnika* **30**(3), 54–61 (2024).
80. Nouh, A. et al. A hybrid of Meta-Heuristic techniques based on cuckoo search and particle swarm optimizations for solar PV systems subjected to partially shaded conditions. *J. Solar Energy Sustain. Dev.* **13**(1), 114–132 (2024).
81. Güven, A. F. & Exploring solar energy systems: A comparative study of optimization algorithms, MPPTs, and controllers. *IET Control Theory Appl.* **18**(7): 887–920 (2024).
82. Kumar, S., Sunil & Balakrishna, K. A novel design and analysis of hybrid fuzzy logic MPPT controller for solar PV system under partial shading conditions. *Sci. Rep.* **14**(1), 10256 (2024).
83. Khan, M. et al. Enhancing efficient solar energy harvesting: a process-in-loop investigation of MPPT control with a novel stochastic algorithm. *Energy Convers. Manage. X* **21**, 100509 (2024).
84. Subbulakshmy, R. et al. Implementation of non-isolated high gain interleaved DC-DC converter for fuel cell electric vehicle using ann-based mppt controller. *Sustainability* **16**(3), 1335 (2024).
85. Wang, H. et al. Theoretical comparison, real-time emulation and experiment validation of DC/DC Converter for Fuel Cell Electric Vehicle. *IEEE Access.* (2024).
86. Aljafari, B. et al. Transformer-less high gain DC–DC converter design and analysis for fuel cell vehicles. *Sci. Rep.* **14**(1), 19221 (2024).

Author contributions

All authors contributed to the study, conception, and design. all authors commented on the manuscript. All

authors read and approved the final manuscript.

Funding
The authors did not receive support from any organization for the submitted work.

Declarations

Competing interests
The authors declare no competing interests.

Ethical approval
This paper does not contain any studies with human participants or animals performed by any of the authors.

Additional information
Correspondence and requests for materials should be addressed to K.B.